

Interaction of oxygen with pristine and defective MoS₂ monolayers

Murilo Kendjy Onita, Flavio Bento de Oliveira, and Andréia Luisa da Rosa*

*Instituto de Física, Universidade Federal de Goiás,
Campus Samambaia, 74690-900, Goiânia, Goiás, Brazil.*

(Dated: January 31, 2023)

Abstract

Atom controlled sub-nanometer MoS₂ pores have been recently fabricated. Oxidative environments are of particular interest for MoS₂ applications in electronics, sensing and energy storage. In this work we carried out first-principles calculations of oxygen adsorption in plain and sub-nanometer MoS₂ nanopores. The chemical stability of the layers and pores towards oxygen was verified using density-functional theory. Dissociation and diffusion barriers have been calculated in order to understand surface and pore oxidation and its electronic properties at the atomic scale.

I. INTRODUCTION

Owing to their fascinating properties, two dimensional transition metal dichalcogenides (TMDs) have been explored for a variety of applications, including electronics and optoelectronics, photonics, catalysis and energy storage¹⁻⁵. In particular, molybdenum disulfide (MoS_2), the most promising TMDCs, is efficiently exfoliated in monolayer or multilayers^{6,7}. Recently the fabrication of MoS_2 sub-nanometer pores offer several opportunities being promising candidates for several technological applications such as membranes for DNA translocation,^{1,8,9} water filtration and desalination¹⁰⁻¹³, energy harvesting¹⁴ and hydrogen evolution reaction¹⁵⁻¹⁷.

Control at atomic scale nanopores can be achieved by using electron or ion beams to fabricate nanopores of specific sizes¹⁸⁻²². Sulfur and molybdenum vacancies, the most abundant defect species in MoS_2 , may serve as the nucleation sites for the nanopore formation^{7,23}. Pore sizes down to 0.5-1.2 nm have been created, corresponding to a few atoms missing²⁴⁻²⁷.

In particular, the interaction of small molecules with MoS_2 is of particular importance, since it plays a role in the properties and performance of two-dimensional-based devices. Concurrently, structural defects such as vacancies and edges are particularly susceptible to attacks in reactive environments²⁸. Adsorption energy and diffusion of oxygen on MoS_2 is controversial and not completely understood. Moreover, oxygen on surfaces either forms undesired alloys entering a sulphur site or possesses a low binding energy. One important, not completely understood question, is the role of point defects on the adsorption of oxygen on MoS_2 . Previous experimental investigations suggested that the presence of defects significantly alters the surface stability^{6,29}. Oxygen leads to the formation of Mo oxide in the two-dimensional MoS_2 lattice, yielding an overall disordered and fragmented structure. On the other hand, other investigations suggested that oxygen is incorporated in the MoS_2 lattice at substitutional sites³⁰. X-ray photoelectron spectroscopy measurements have shown that the basal plane of MoS_2 monolayers, when subjected to long-term ambient exposure, spontaneously undergoes oxygen substitution reactions, giving rise to a highly crystalline two-dimensional molybdenum oxysulfide phase^{31,32}.

In this work we have investigated the interaction of oxygen atoms and molecules with MoS_2 monolayers and subnanometer pores. The pore size and termination play a crucial role on the interaction with oxygen molecules.

II. METHODOLOGY

All calculation have been performed using the density functional theory^{33,34} as implemented in the VASP³⁵. For the exchange-correlation functional we use the GGA approximation³⁶. Basis set consisting of an expansion in plane waves and an energy cutoff of 300 eV were used. The Brillouin zone was sampled according to the Monkhorst-Pack scheme³⁷ with Γ point only in a (6×6) unit cells. To avoid interaction between neighbouring wires, a vacuum space of 15 Å was set in the direction perpendicular to the two-dimensional MoS₂ layers. The structural relaxation was performed until the atomic forces were less than 10^{-3} eV/Å. In order to determine the diffusion and reaction barriers we have performed CI-NEB^{38,39} calculations with at least seven images to search the minimum-energy reaction paths and saddle points between the initial state and final state configurations.

III. RESULTS

Among the various arrangements for MoS₂, the energetically most stable one at room temperature is known as 2H which has a honeycomb structure as shown in Fig.1 (a) and (b). This arrangement has in its unit cell one molybdenum and two sulfur atoms. The optimized Mo-S (S-S) distances are 2.42 (3.14) Å. The lattice parameter $a = b$ equals to 3.16 Å. The electronic band structure and total density-of-states (DOS) of bare a MoS₂ monolayer are shown in Fig.1(b). The direct band gap at K-point is 1.76 eV, in agreement with previous results⁴⁰.

The electronic band gap and formation energies of bare and defective monolayered MoS₂ are reported in our previous publication⁴¹. The formation enthalpy of a bare MoS₂ monolayer is -2.63 eV.

Here the adsorption energy of oxygen is calculated at high oxygen chemical potential according to: $E_b = E_{\text{MoS}_2/\text{O}} - E_{\text{MoS}_2\text{-bare}} - \sum_i \mu_{\text{O}}$, where $E_{\text{MoS}_2/\text{O}}$ is the total energy of the MoS₂ the with oxygen adsorbed, $E_{\text{MoS}_2}^{\text{bare}}$ is the total energy of the bare sheet, μ_{O} is the chemical potential of oxygen, which has ben chosen as the total energy of the oxygen molecule.

As possible configurations for defective MoS₂, we have considered oxygen substituting sulphur atoms, namely O_S, with concentrations of 11%, 22% and 25% as shown in Figs.2

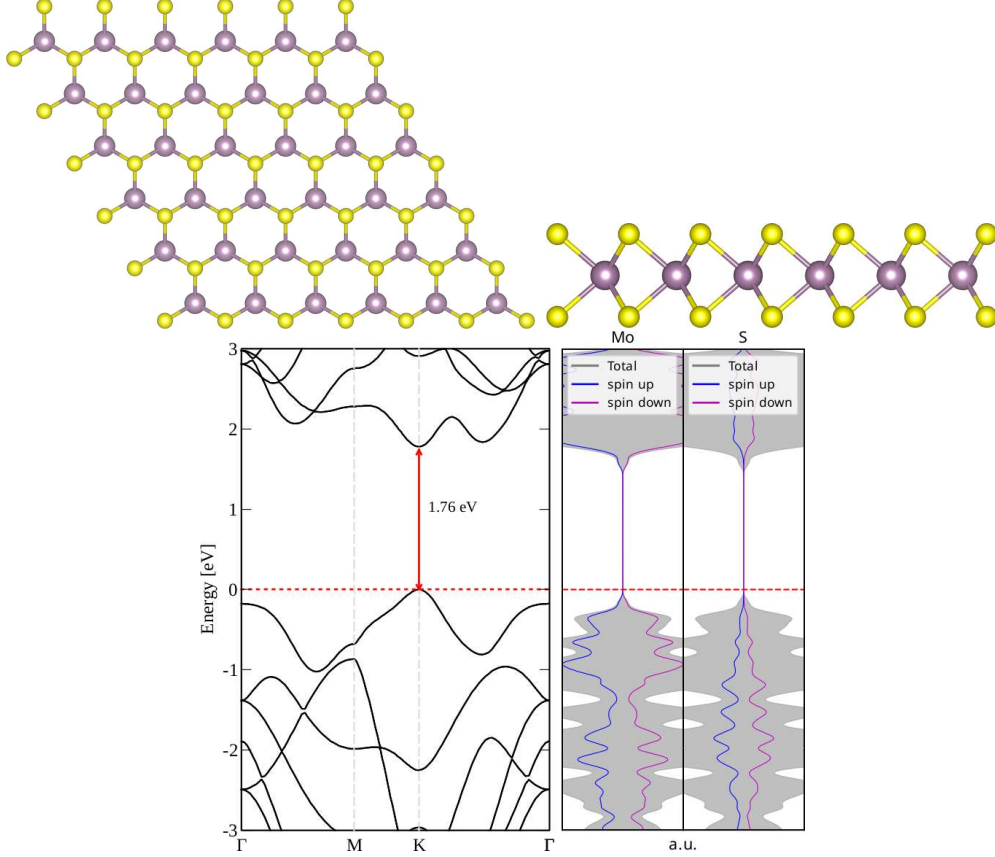


FIG. 1 a) Top view, b) side view and c) electronic band structure and DOS of bare MoS₂ monolayers.

(a), (b) and (c), respectively. We notice that substitution at Mo sites is highly unfavorable. Furthermore, defects have been incorporated considering Mo vacancies namely O_S (11%) + V_{Mo}, Fig.2 (d) and S vacancies, Figs.2 (e) and (f) labeled as O_S (11%) + V_S (far) and O_S (11%) + V_S (close). These concentrations were chosen based on experimental results reported in Ref. ⁴². We have included disorder effects by adding Mo vacancies far and close to oxygen substitutional atoms, as mentioned above.

In Fig.3 the DOS and PDOS of the oxygen substitutional in MoS₂ is shown. a) O_S at (11%), b) O_S at (22%), c) O_S (25%), d) O_S^{close} + V_{Mo} (11%), e) O_S^{far} + V_{Mo} (11%), f) O_S^{close} + V_S (11%). The electronic structure of a) O_S at (11%), b) O_S at (22%) is very similar. The later two systems exhibit semiconductor behavior.

At higher concentration as in O_S (25%), Fig.3(c), additional state in the gap appear, but the structure remain semiconducting. For d) O_S^{close} + V_{Mo} (11%) and O_S^{far} + V_{Mo} (11%) states cross the Fermi level, indicating a metallic behavior. Finally, for O_S^{close} + V_S (11%)

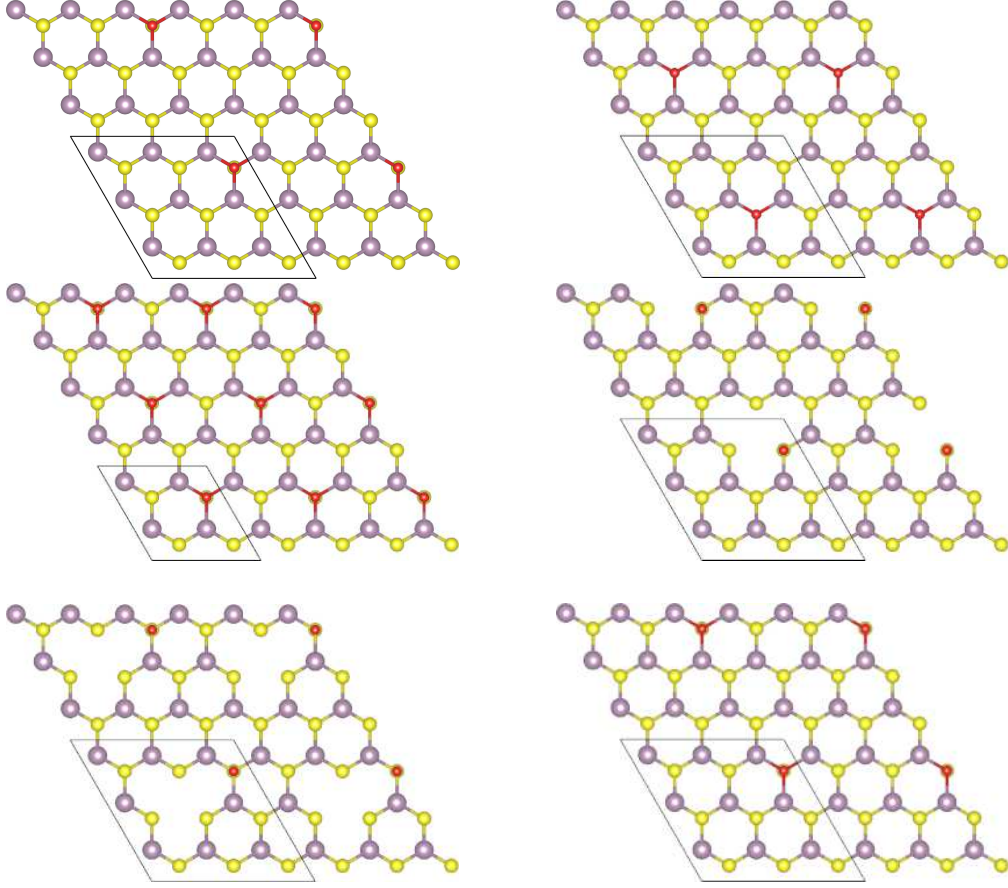


FIG. 2 Relaxed structure of oxygen substitutional in MoS₂ nanopores. a) O_S (11%), b) O_S (22%), c) O_S (25%), d) O_S (11%) + V_{Mo}, e) O_S (11%) + V_S (far) and f) O_S (11%) + V_S (close). Purple, yellow and red are Mo, S and O atoms, respectively. The oxygen concentration is given within brackets.

shown in Fig. 3(f) the system is a semiconductor as well.

TABLE I Binding energies of oxygen molecules in MoS₂ nanopores.

Structure	E _b (eV)
pristine	-0.55
V _{1Mo} -O ₂ (non-diss.)	-0.37
V _{1S} -O ₂ (diss.)	-0.90
V _{2S} -O ₂ (diss.)	-3.44
V _{1Mo6S-3O₂} (diss.)	-3.24
V _{1Mo6S-O₂} (non-diss.)	-0.45

On the monolayer pristine the oxygen molecule spontaneously dissociates and the oxygen atoms diffuses further apart to finally bind on the sulfur atoms. This means that the barrier

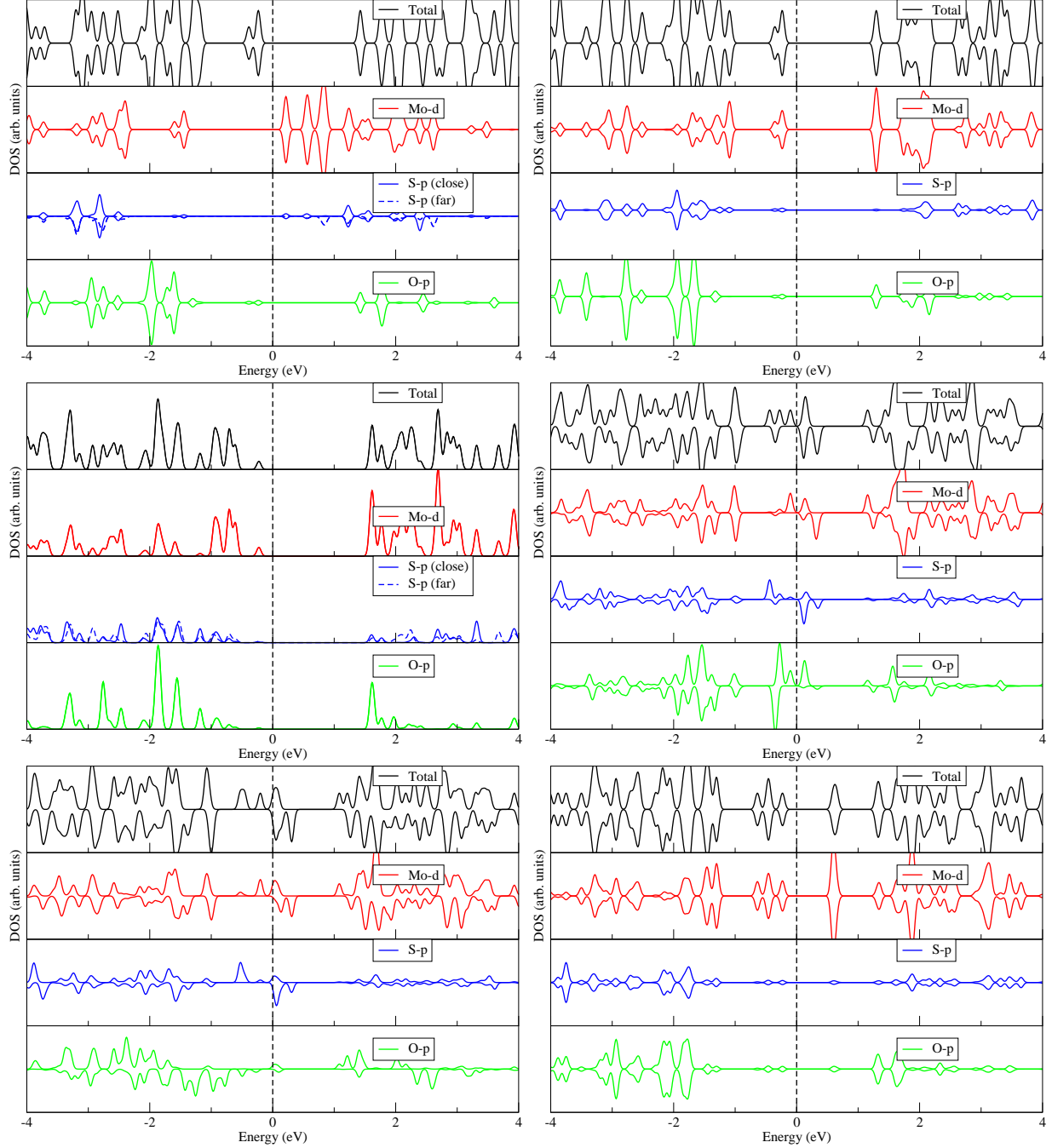


FIG. 3 DOS and PDOS of O_S in MoS_2 nanosheets at different oxygen concentrations: a) O_S at (11%), b) O_S at (22%), c) O_S (25%), d) $O_S^{\text{close}} + V_{Mo}$ (11%), e) $O_S^{\text{far}} + V_{Mo}$ (11%), f) $O_S^{\text{close}} + V_S$ (11%).

for O diffusion should be low, as suggested in Ref.⁴³. The binding energy of the final configuration is -1.13 eV/atom. In addition we have investigated the interaction of O_2 with other small defects which we call subnanometer pores: a Mo single vacancy, V_{Mo-O_2} , shown

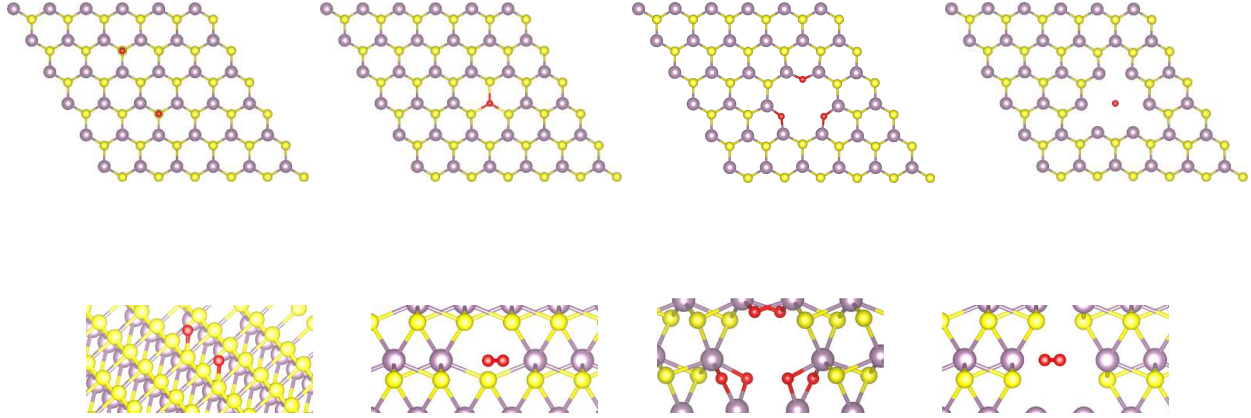


FIG. 4 Top and rotated views of relaxed structures of oxygen adsorption in MoS₂ monolayers. a) and e) pristine, b) and f) V_{1Mo}-O₂, c) and g) V_{1Mo6S}-3O₂ (dissociated) and d) and h) V_{1Mo6S}-O₂ (non-dissociated) defects.

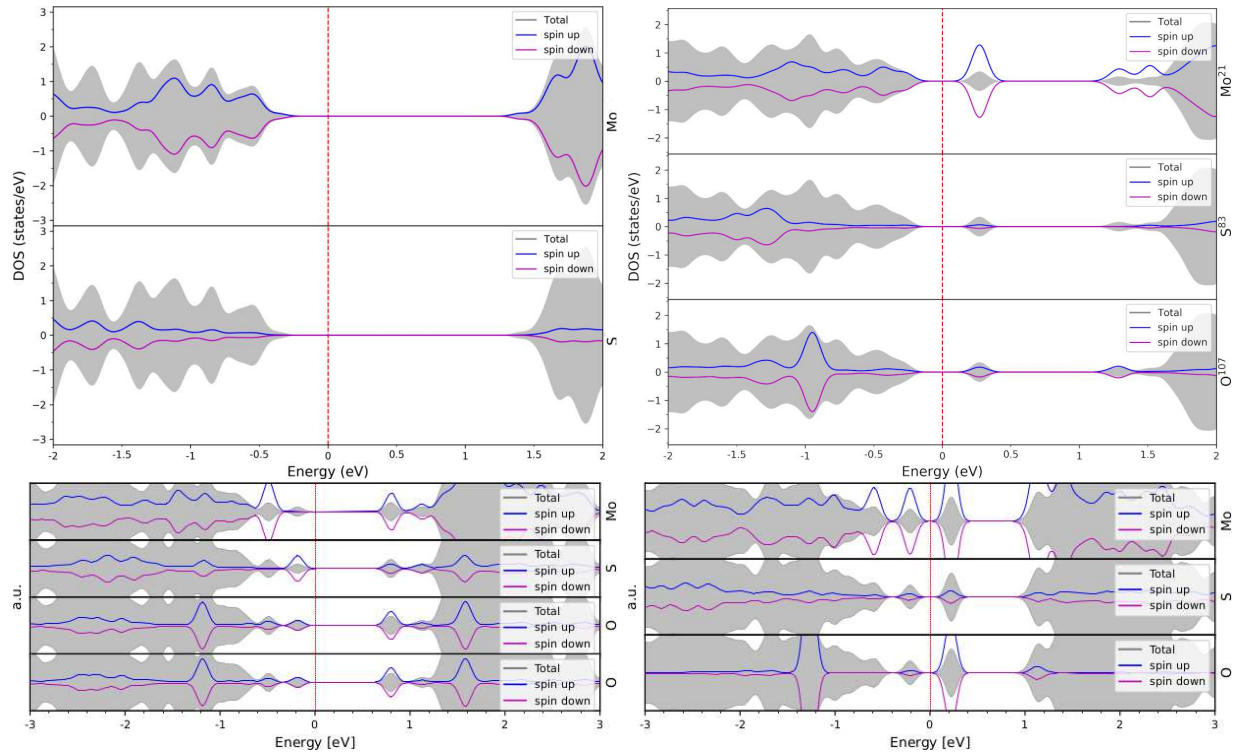


FIG. 5 DOS and PDOS of oxygen adsorbed in MoS₂ monolayers: a) pristine and with b) V_{1Mo}-O₂, c) V_{1Mo6S}-3O₂ (dissociated), d) V_{1Mo6S}-O₂ (non-dissociated) defects.

in Fig. 4 (b), a Mo single vacancy plus S hexavacancy, V_{1Mo6S}-O₂, shown in Fig. 4 (c) and d) V_{1Mo6S}-O₂ (non-dissociated). Such structures can serve as prototypes for nanopores in MoS₂. Additionally, we have considered a Mo triple vacancy plus a S divacancy, V_{3Mo2S}-O₂,

and a single Mo vacancy plus a S tetravacancy, $V_{1\text{Mo}4\text{S}-\text{O}_2}$, a Mo triple vacancy plus a S hexavacancy, $V_{3\text{Mo}6\text{S}-\text{O}_2}$ (to be published).

Binding energies of oxygen for the relaxed structures are shown in Table I. On pristine MoS_2 , shown in Fig. 4 (a), adsorption of oxygen leads to a dissociative configuration with binding energy is -0.55 eV/O atom . Oxygen spontaneously dissociates with the oxygen atoms diffusing further apart with a 6.3 \AA being the smallest O-O distance. The O sits right above the S atom with S-O distance equal to 1.48 \AA .

On $V_{1\text{Mo}-\text{O}_2}$ oxygen chemisorbs in a non-dissociate manner with binding energy of -0.37 eV/O atom . The O-O distance is 2.78 \AA with each oxygen bound to a sulphur atom in different layers. The relaxed geometry is shown in Fig. 4 (b).

In a single sulfur vacancy defect, $V_{1\text{S}-\text{O}_2}$, shown in Fig. 4 (c), the oxygen molecule dissociates. Upon dissociation, the first atom goes to a substitutional sulphur site, while the second oxygen atom moves to ontop of a sulphur atom. This is in agreement with results reported previously⁴⁴. The binding energy is -0.90 eV/O atom .

On a double sulphur vacancy, $V_{2\text{S}-\text{O}_2}$ both oxygen atoms go to substitutional sulphur positions. The Mo-O bond length is 1.7 \AA forming a slightly distorted hexagon. One notes that typical Mo-O bond lengths range from 1.69 to 1.73 \AA ⁴⁵. The O-O distance is our case 2.38 \AA . The binding energy amounts -3.44 eV/atom , meaning that the reaction is exothermic.

The $V_{1\text{Mo}6\text{S}-\text{O}_2}$ interacts with the oxygen molecule via a perpendicular orientation of the molecule with respect to the MoS_2 surface in its final configuration. The oxygen distance to the molybdenum atoms is around 3 \AA .

For other large nanopores such as $V_{3\text{Mo}6\text{S}-\text{O}_2}$, $V_{1\text{Mo}4\text{S}-\text{O}_2}$ and $V_{3\text{Mo}2\text{S}-\text{O}_2}$ (to be published), the binding energy indicates physisorption, with the O_2 molecule lying in the middle of the pore with O-O bond distance equals to 1.0 \AA . We may argue here that there is an interplay between the number of oxygen atoms and the number of dangling bonds in the pore.

The density of states of the above discussed nanopores are show in Fig. 5. $V_{1\text{S}-\text{O}_2}$ shows states within the gap, as seen in Fig. 5(a). On the other hand, $V_{2\text{S}-\text{O}_2}$ does not have states in the gap as shown in Fig. 5(b). Furthermore, $V_{1\text{Mo}-\text{O}_2}$ and $V_{1\text{Mo}6\text{S}-\text{O}_2}$ have states within the gap due to sulphur dangling bonds.

Recently it has been suggested that the formation of oxygen at substitutional sites with no band gap states can be formed in MoS_2 layers⁴². A possible explanation for the ordered oxygen incorporation is that due to the higher strength of the Mo-O bonds compared to M-S,

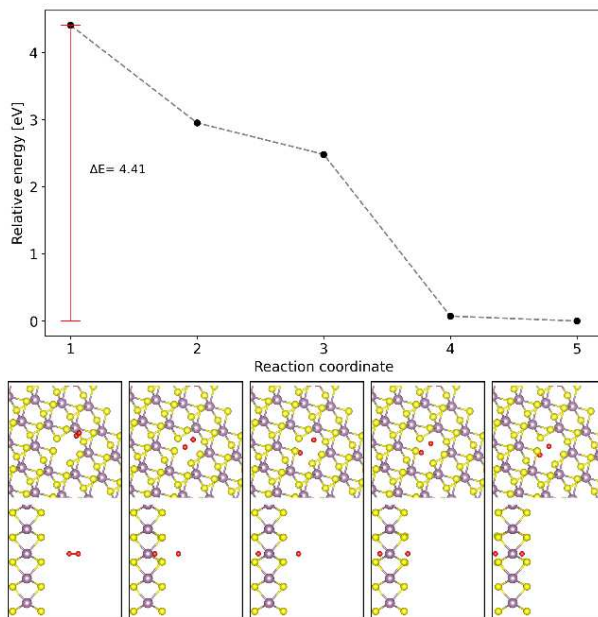


FIG. 6 Diffusion barrier (top panel) and corresponding paths (lower panel) of an oxygen molecule on a molibdenum vacancy in MoS_2 with perpendicular orientation to the MoS_2 basal plane.

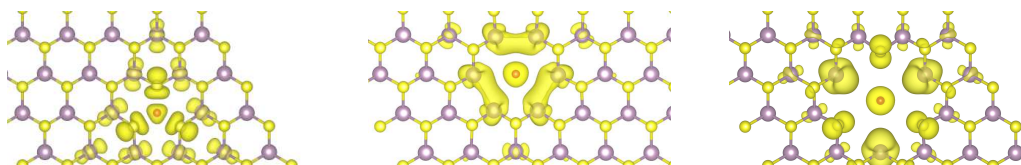


FIG. 7 Projected charge density on LUMO-1 of a) $\text{V}_{1\text{Mo}}-\text{O}_2$, b) $\text{V}_{1\text{Mo}6\text{S}}-\text{O}_2$ and c) $\text{V}_{3\text{Mo}6\text{S}}-\text{O}_2$. Isosurface value is $0.003 \text{ e}/\text{bohr}^3$

the substitutional oxidation of the 2D MoS_2 basal plane could be also thermodynamically favourable^{29,46}. One can explain the dissociation considering that SO_2 has cohesive energy of -3.1 eV , which is larger than the formation enthalpy of MoS_2 which is -2.48 eV .

Experiments reveal relatively low activation energy values for MoS_2 oxidation, ranging from 0.54 eV to 0.98 eV ⁴³. Recent theoretical calculations⁴⁴ report a barrier of 0.33 eV in the presence of sulphur defects. Here we considered the presence of a molibdenum vacancy. The reaction path is done by following the molecule along its minimum energy path. We have used between five and eight intermediate states to calculate the diffusion. While oxygen atom diffuses through the pore with a barrier of 2.53 eV . On the other hand, an oxygen molecule diffuses barrierless along the path shown in Fig. 6 respectively.

In order to have further insight on the interaction between the oxygen molecules and the

nanopores we have calculated the projected partial charge density on the first level above the Fermi level. These are shown in Fig. 7 (a) for $V_{1\text{Mo}-\text{O}_2}$ which has the unoccupied orbitals of the pore oriented towards the molecule. However, as the preferred orientation of the molecule in the middle of the pore is perpendicular to the pore, this could explain the small overlap between HOMO of the molecule and LUMO of the pore and therefore the relative small barrier for $V_{1\text{Mo}-\text{O}_2}$ where the molecule easily diffuses through the pore.

For the $V_{1\text{Mo}-\text{O}_2}$ the molecule diffuses without barrier. Furthermore, the $V_{3\text{Mo}_6\text{S}-\text{O}_2}$ pore is large enough for the molecule to diffuse either parallel or perpendicular to the pore. However, if the molecule is close enough to the edges, it is likely to dissociate. On the other hand, the $V_{1\text{Mo}_6\text{S}-\text{O}_2}$ pore have its Mo orbitals hybridizing forming metallic-like bonds.

IV. CONCLUSIONS

In this work we carried out first-principles calculations of oxygen on monolayered MoS_2 and sub-nanometer MoS_2 nanopores. The dissociation and diffusion of oxygen in MoS_2 reveal two main features: the orientation of the molecule with respect to the surface plays a role on the molecule diffusion barrier; the reactivity of the pore plays a role on the molecule dissociation.

V. ACKNOWLEDGEMENTS

We acknowledge financial support from Conselho Nacional de Pesquisa e Desenvolvimento (CNPq) under grants 313081/2017-4 and 305335/2020-0. The calculations have been performed using the computational facilities of Santos Dumont Supercomputar at LNCC, CENAPAD at Unicamp and LaMCAD/UFG.

* andreialuisa@ufg.br

¹ J. Feng, K. Liu, R. D. Bulushev, S. Khlybov, D. Dumcenco, A. Kis, and A. Radenovic, *Nat. Nanotechnol.* **10**, 1070 (2015).

² J. Feng, M. Graf, K. Liu, and D. Ovchinnikov, *Nature* **536**, 7615 (2016).

³ J. Feng, M. Graf, and K. e. a. Liu, *Nature* **536**, 197 (2016).

- ⁴ N. Karmodak, L. Bursi, and O. Andreussi, *The Journal of Physical Chemistry Letters* **13**, 58 (2021).
- ⁵ B. Chamlagain and S. I. Khondaker, *ACS Omega* **6**, 24075–24081 (20x).
- ⁶ K. C. Santosh, R. C. Longo, R. M. Wallace, and K. Cho, *J. Appl. Phys.* **117**, 135301 (2015).
- ⁷ C. Tsai, H. Li, S. Park, J. Park, H. S. Han, J. K. Norskov, X. Zheng, and F. A.-Pedersen, *Nat. Commun.* **8**, 15113 (2017).
- ⁸ P. Sen and M. Gupta, *RSC Advances* **11**, 6114 (2021).
- ⁹ M. Graf, M. Lihter, D. Altus, S. Marion, and A. Radenovic, *Nano Lett.* p. 9075 (2019).
- ¹⁰ Z. Cao, V. Liu, and A. B. Farimani, *ACS Energy Lett.* **5**, 2217 (2020).
- ¹¹ J. Kou, J. Yao, L. Wu, X. Zhou, H. Lu, F. Wu, and J. Fan, *Phys. Chem. Chem. Phys.* **18**, 22210 (2016).
- ¹² M. Heiranian, A. B. Farimani, and N. R. Aluru, *Nat. Comm.* **6**, 8616 (2015).
- ¹³ L. Wang, Z. Wang, S. K. Patel, S. Lin, and M. Elimelech, *ACS Nano* **15**, 4093 (2021).
- ¹⁴ M. Graf, M. Lihter, D. Unuchek, A. Sarathy, J.-P. Leburton, A. Kis, and A. Radenovic, *Joule* **3**, 1549 (2019).
- ¹⁵ L. Wu, A. Longo, N. Y. Dzade, A. Sharma, M. M. R. M. Hendrix, A. A. Bol, N. H. de Leeuw, E. J. M. Hensen, and J. P. Hofmann, *ChemSusChem* **12**, 4383 (2019).
- ¹⁶ W. Li, G. Liu, J. Li, Y. Wang, L. Ricardez-Sandoval, Y. Zhang, and Z. Zhang, *Appl. Surf. Sci.* **498**, 143869 (2019).
- ¹⁷ J. Xu, G. Shao, X. Tang, F. Lv, H. Xiang, C. Jing, S. Liu, S. Dai, Y. Li, J. Luo, et al., *Nature Communications* **13**, 219 (2022).
- ¹⁸ C.-H. Chen, X. Chang, and C.-S. Wu, *Sci. Rep.* **9**, 18663 (2019).
- ¹⁹ W. Shi, A. K. Friedman, and L. A. Baker, *Anal. Chem* **89**, 157 (2017).
- ²⁰ D. Garoli, H. Yamazaki, N. Maccaferri, and M. Wanunu (2019).
- ²¹ J. Lin, O. Cretu, W. Zhou, K. Suenaga, D. Prasai, K. I. Bolotin, N. Y. Cuong, M. Otani, S. Okada, A. R. Lupini, et al., *Nat. Nanotech.* (2014).
- ²² P. Vancsó, G. Z. Magda, J. Petö, J.-Y. Noh, Y.-S. Kim, C. Hwang, and dL. Tapasztó, *Sci. Rep.* **6**, 29726 (2016).
- ²³ D. J. Trainer, J. Nieminen, F. Bobba, B. Wang, X. Xi, A. Bansil, and M. Iavarone, *2D Materials and Applications* **6**, 13 (2022).

- ²⁴ X. Zhao, D. Fu, Z. Ding, Y. Zhang, D. Wan, S. J. R. Tan, Z. Chen, K. Leng, J. Dan, W. Fu, et al., *Nano Lett.* **18**, 482 (2018).
- ²⁵ S. Wang, H. Li, H. Sawada, C. S. Allen, A. I. Kirkland, J. C. Grossman, and J. H. Warner, *Nanoscale* **9**, 6417 (2017).
- ²⁶ J. P. Thiruraman, P. M. Das, and M. Drndić, *ACS Nano* **14**, 11831 (2020).
- ²⁷ K. Yin, S. Huang, X. Chen, X. Wang, J. Kong, Y. Chen, and J. Xue, *ACS Appl. Mater. Interfaces* p. 28909 (2018).
- ²⁸ T. Gruenleitner, A. Henning, M. Bissolo, M. Zengerle, L. Gregoratti, M. Amati, P. Zeller, J. Eichhorn, A. V. Stier, A. W. Holleitner, et al., *ACS Nano* **16**, 20364–20375 (2022).
- ²⁹ R. C. Longo, R. Addou, K. C. Santosh, J.-Y. Noh, C. M. Smyth, D. Barrera, C. Zhang, J. W. P. Hsu, R. M. Wallace, and K. Cho, *2D Materials* **4**, 025050 (2017).
- ³⁰ M. H. Jeon, C. Ahn, H. Kim, K. N. Kim, T. Z. Li, H. Qin, Y. Kim, S. Lee, T. Kim, and G. Y. Yeo, *Nanotechnology* **26**, 355706 (2015).
- ³¹ J. Petö, T. Ollár, P. Vancsó, Z. I. Popov, G. Z. Magda, G. Dobrik, C. Hwang, P. B. Sorokin, and L. Tapasztó, *Nature Chem.* **10**, 1246 (2018).
- ³² M. Chhowalla, H. S. Shin, G. Eda, L.-J. Li, K. P. Loh, and H. Zhang, *Nature Chem.* **5**, 263 (2013).
- ³³ P. Hohenberg and W. Kohn, *Phys. Rev.* **136**, B864 (1964).
- ³⁴ W. Kohn and L. J. Sham, *Phys. Rev.* **140**, A1133 (1965).
- ³⁵ G. Kresse and D. Joubert, *Phys. Rev. B* **59**, 1758 (1999).
- ³⁶ J. P. Perdew, K. Burke, and M. Ernzerhof, *Phys. Rev. Lett.* **77**, 3865 (1996).
- ³⁷ H. J. Monkhorst and J. D. Pack, *Phys. Rev. B* **13**, 5188 (1976).
- ³⁸ H. Henkelman, G.; Jónsson, *J. Chem. Phys.* **113** (2000).
- ³⁹ H. Henkelman, G.; Jónsson, *J. Chem. Phys.* **113**, 9978–9985 (2000).
- ⁴⁰ H.-P. Komsa and A. V. Krasheninnikov, *Phys. Rev. B* (2015).
- ⁴¹ M. Kendjy, A. L. da Rosa, and T. Frauenheim, **34**, 044005 (2022).
- ⁴² J. Tang, Z. Wei, Q. Wang, Y. Wang, B. Han, X. Li, B. Huang, M. Liao, J. Liu, N. Li, et al., *Small* **16**, 2004276 (2020).
- ⁴³ R. Rao, A. E. Islam, P. M. Campbell, E. M. Vogel, and B. Maruyama, *2D materials* **4**, 025058 (2017).
- ⁴⁴ K. Wang and V. Paulus, *J. Phys. Chem. C* **125**, 19544–19550 (2021).

⁴⁵ F. D. Hardcastle and I. E. Wachs, *J. Raman Spectroscopy* **21**, 683 (1990).

⁴⁶ J. Martinová, M. Otyepka, and P. Lazar, **23**, 13233 (2017).